

1 **Supplementary material of**  
2 **New insights into active tectonics and seismogenic potential of the Italian Southern Alps from**  
3 **vertical geodetic velocities**

4

5

6 Letizia Anderlini<sup>1\*</sup>, Enrico Serpelloni<sup>2</sup>, Cristiano Tolomei<sup>2</sup>, Paolo Marco De Martini<sup>2</sup>, Giuseppe  
7 Pezzo<sup>2</sup>, Adriano Gualandi<sup>3</sup>, Giorgio Spada<sup>4</sup>

8

9 <sup>1)</sup> Istituto Nazionale di Geofisica e Vulcanologia, Bologna (Italy)

10 <sup>2)</sup> Istituto Nazionale di Geofisica e Vulcanologia, Rome (Italy)

11 <sup>3)</sup> Jet Propulsion Laboratory, California Institute of Technology (USA)

12 <sup>4)</sup> DiSPeA, Urbino University (Italy)

13

14

15

16 **Text S1 - S3**

17 **Figures S1 - S7**

18 **Tables S1 - S3**

19 **References**

20

## 21 **Text S1. GPS Data Processing**

22 The position time-series have been obtained adopting a three-step procedure approach, as in  
23 Serpelloni et al. (2006), that includes: 1) raw phase data reduction, 2) combination of loosely  
24 constrained network solutions and reference frame definition and 3) time-series analysis, including  
25 velocity estimates and spatial filtering of common mode errors.

26 The raw GPS observables have been analyzed using the 10.6 version of the GAMIT/GLOBK package  
27 (Herring et al., 2015) adopting standards defined in the framework of the IGS “Repro2 campaign”  
28 (<http://acc.igs.org/reprocess2.html>). The GAMIT software is used to estimate station positions,  
29 atmospheric delays, satellite orbits, and Earth orientation parameters from ionosphere-free linear  
30 combination GPS phase observables using double differencing techniques to eliminate phase biases  
31 caused by drifts in the satellite and receiver clock oscillators. GPS pseudo-range observables are used  
32 to constrain clock timing offsets and to improve automated editing of the phase data, assisting in the  
33 resolution of integer phase ambiguities. GPS phase data are weighted according to an elevation-angle-  
34 dependent error model (Herring et al., 2015) using an iterative analysis procedure whereby the  
35 elevation dependence is determined from the observed scatter of phase residuals.

36 In this analysis the satellites orbit parameters are fixed to the IGS final products. We use the IGS  
37 absolute antenna phase center model for both satellite and ground- based antennas, which improves  
38 the accuracy of estimates for the vertical components of site position by mitigating reference frame  
39 scale and atmospheric mapping function errors (e.g., Schmid et al., 2005, 2007). While the first-order  
40 ionospheric delay is eliminated by the ionosphere-free linear combination, the second-order  
41 ionospheric corrections are applied based on the formulation of Petrie et al. (2010), using IONEX  
42 files from the Center for Orbit Determination in Europe (CODE). The tropospheric delay is modeled  
43 as piecewise linear model and estimated using the Vienna Mapping Function 1 (VMF1; Boehm et al.,  
44 2006) with a 10° cutoff. We use the Global Pressure and Temperature 2 (GPT2; Lagler et al., 2013)  
45 model to provide a priori hydrostatic delays. The pole tide was also corrected in GAMIT by IERS  
46 standards. The Earth Orientation Parameters (EOP) are tightly constrained to priori values obtained  
47 from IERS Bulletin B. Non-tidal atmospheric loading and ocean tidal loading are corrected using  
48 MIT filtered atmospheric displacements files (available at <ftp://everest.mit.edu/pub/GRIDS>) and the  
49 FES2004 (Lyard et al., 2006) model, respectively. The International Earth Rotation Service (IERS)  
50 2003 model for diurnal and semi-diurnal solid Earth tides was set.

51 Because of the large number of stations included in our Euro-Mediterranean GPS processing (~3000),  
52 this step is performed for several sub-networks, each made by <50 stations, with each sub-network  
53 sharing a set of high-quality IGS stations, which are used as tie-stations in the combination step.

54 In the second step we use the ST\_FILTER program of the QOCA software (<http://qoca.jpl.nasa.gov>),  
55 which adopts a Kalman filter estimation algorithm (Dong et al., 1998, 2002), to combine all the daily

56 loosely constrained solutions with the global solution of the IGS network made available by MIT  
57 (<http://sopac.ucsd.edu>), and simultaneously realize a global reference frame by applying generalized  
58 constraints (Dong et al., 1998). Specifically, we define the reference frame by minimizing the  
59 velocities of the IGS core stations (<http://igs.cb.jpl.nasa.gov>), while estimating a seven- parameter  
60 transformation with respect to the GPS realization of the ITRF2008 frame (Altamimi et al., 2011),  
61 i.e., the IGB08 reference frame.

62 In the third step we analyze the position time series in order to estimate and correct offsets due to  
63 stations equipment changes, while simultaneously estimating annual and semi-annual periodic signals  
64 and a linear velocity term. In this analysis we retain only data from GPS stations with an observation  
65 period longer than 2.5 years, as shorter intervals may result in biased estimates of linear velocities  
66 (Blewitt and Lavallée, 2002). The model derived from the combination of these signals is then  
67 subtracted from the position time series in order to get the residual positions. The residual time-series  
68 are then used to estimate the Common Mode Error (CME) performing a Principal Component  
69 Analysis (PCA), as described in Dong et al. (2006). The PCA is performed at a continental-scale,  
70 over the same area used by Serpelloni et al. (2013), and the first two PCs are here considered as CME.  
71 This prevents the removal of the eventual more localized signals of geophysical interests recorded by  
72 the GPS stations in the study region, since the PCA detects the signals common to a much larger  
73 region. As a result, after removing the CME, the typical repeatability in our analysis is  $\sim 1$  mm for the  
74 horizontal components, and  $\sim 3$  mm for the vertical component, with a 30% gain in the daily  
75 repeatability and a significant improvement of the signal to noise ratio. After the spatial filtering, the  
76 estimated seasonal motions are added back to the filtered time-series, obtaining position time series  
77 with a reduced scatter around the adopted model.

78

## 79 **Text S2. Vertical Leveling Data**

80 The IGMI leveling campaigns have been performed following the International Geodetic Association  
81 standards defined in Oslo in 1948 (Vignal, 1936; 1950) that allows to have a high level accuracy of  
82 the final vertical rates. The considered leveling line is composed by almost a hundred benchmarks  
83 starting from the fixed one in Mestre (Venice) moving northward up to Fadalto valley and Val Belluna  
84 within the Venetian Eastern Southern Alps. The elevation changes measured during the campaign  
85 time interval (1952-1984) are reported in Table S2 along with the distance with respect to the  
86 reference benchmark and the position of each one in latitude and longitude. The available information  
87 on the levelling campaigns are only in terms of the final estimates of elevation values for each  
88 benchmark, without any notes about the discrepancy value obtained between forward and backward  
89 levelling measurements line, about the presence of any systematic errors and if any adjustment or  
90 correction has been applied during measurements procedures. In order to evaluate a reliable error

91 associated with the elevation change estimate, we use the formula proposed by D’Anastasio et al.  
92 (2006):

$$93 \quad e_i = \pm \sqrt{2 \sum_{j=1}^i (\sigma \sqrt{l_j})^2}$$

94 where  $l_i$  is the distance (in km) between consecutive benchmarks (thus  $\sum_{j=1}^i l_j = L_i$  indicates the  
95 distance of each benchmark from the reference one) and  $\sigma$  is the maximum allowed discrepancy  
96 between forward and backward levelling line standard error of a 1 km long levelled segment, for  
97 which we use the value of  $2.5 \text{ mm}/\sqrt{\text{km}}$  (D’Anastasio et al., 2006). The propagated error  $e_i$  indicates  
98 the error between the fixed benchmark and the  $i$ -th benchmark, representing the maximum allowable  
99 random error propagation (D’Anastasio et al., 2006). The propagated error is graphically depicted in  
100 Fig. S3A with the two continuous curves that allow to evaluate which elevation changes can be  
101 considered significant with respect to this maximum allowable random error. The error of the  
102 elevation change rate has been calculated considering the time interval of measurements ( $\Delta t = 32$   
103 years) as follows:  $e_{ECi} = e_i/\Delta t$  (see Table S2 and Figure S3B).

104

105

### 106 **Text S3. Subsampling InSAR data method**

107 The method used to subsample InSAR datasets is based on the pixel density. The number of InSAR  
108 pixel is reduced maintaining the information of deformation provided by the original velocity field.  
109 We take into account the original area covered by the InSAR frame as the rectangle identified by the  
110 minimum and maximum values of latitude and longitude of InSAR pixels. We subdivide this  
111 rectangle into sub-portions until within each one there’s a number of pixel lower than a reference one,  
112  $n_{crit}$ . At this point each sub-portion is represented by just one pixel whose associated longitude,  
113 latitude and velocity are calculated as the median values of the enclosed pixels. The subsampling has  
114 been performed for both the ascending and descending solutions just on a portion of the InSAR  
115 dataset that is a 35 km wide stripe across the Montello and Bassano-Valdobbiadene thrusts along the  
116 NNW direction (see Figure S4). Considering two iterations of subdivisions, we define the number of  
117 divisions along longitude and latitude assuming two parameters:

- 118 1. the final number of pixel we want to obtain after the subsampling,  $Np$ ;
- 119 2. the percentage of area,  $R$ , covered by the original InSAR data with respect to the initial  
120 rectangle.

121 For the first parameter we considered the same number for both datasets in order to do not have any  
122 predominance of one to the other, and to have a final dataset of few thousands of points that do not

123 generate too much high computational costs. The second value is a more empirical estimate that could  
124 vary from 20% to 45%. The two parameters are related to each other in order to define the total  
125 number of subcells at the end of the two iterations. This means that if we want  $N_p$  final points for an  
126 initial dataset that covers the starting region of  $R$  percentage, the subdivision along longitude ( $div_{lon}$ )  
127 and along latitude ( $div_{lat}$ ) are such that the following relation is valid:

$$128 \quad \frac{N_p}{R} = (div_{lon} * div_{lat})^2$$

129 Along this rationale, we define the two parameters  $div_{lon}$  and  $div_{lat}$  by trial and error in order to get  
130 the most equal number  $N_p$  possible for the two datasets. For each settled  $div_{lon}$  and  $div_{lat}$  we define  
131 the critical number of pixel,  $n_{crit}$ , below which the cell is not further subdivided, as follows:

$$132 \quad n_{crit} = \frac{T_p}{div_{lon} * div_{lat}}$$

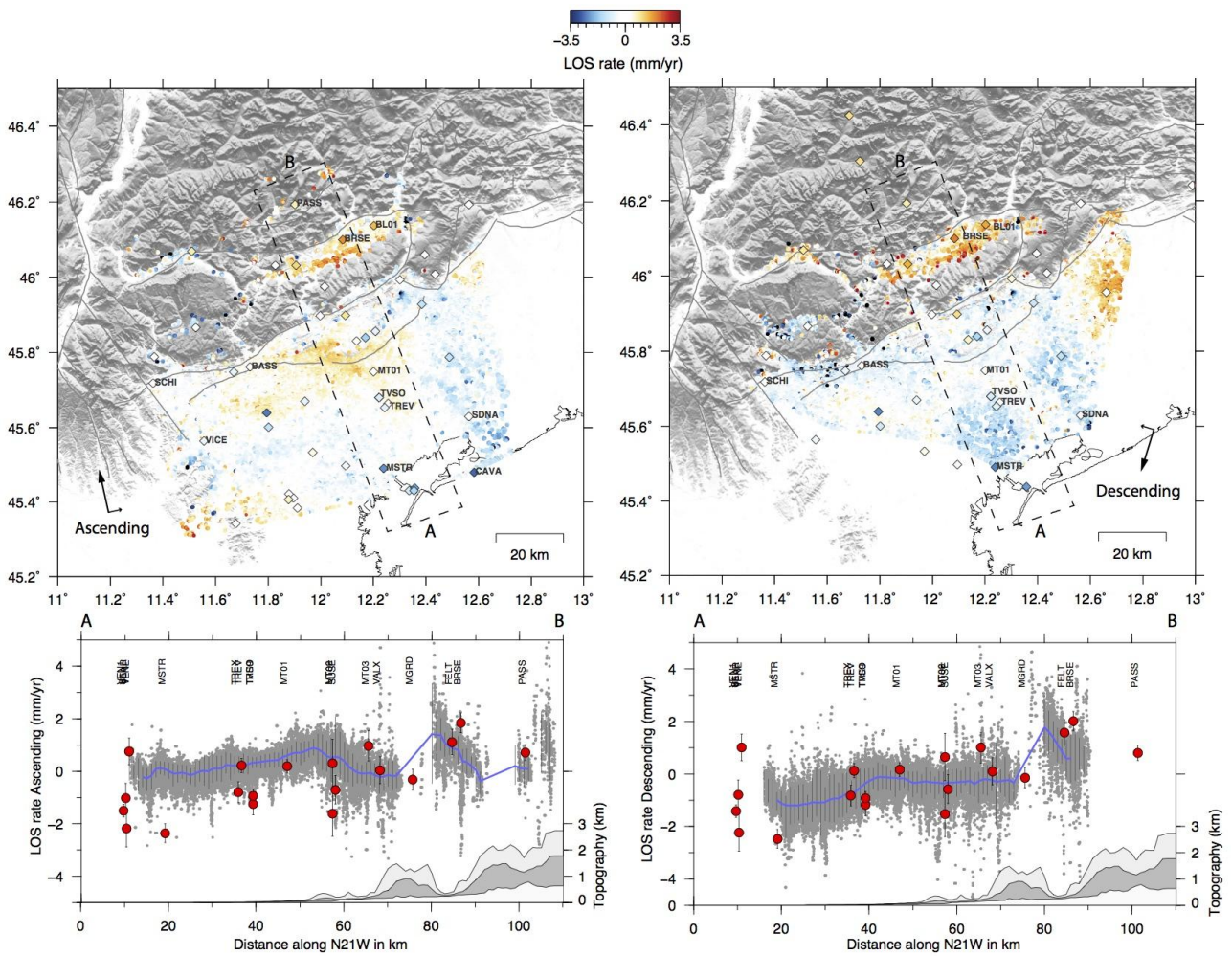
133 where  $T_p$  indicates the initial number of pixel of the InSAR dataset.

134 The specific parameters considered in each subsampling for both the ascending and descending  
135 datasets are reported in Table S3.

136

137

138

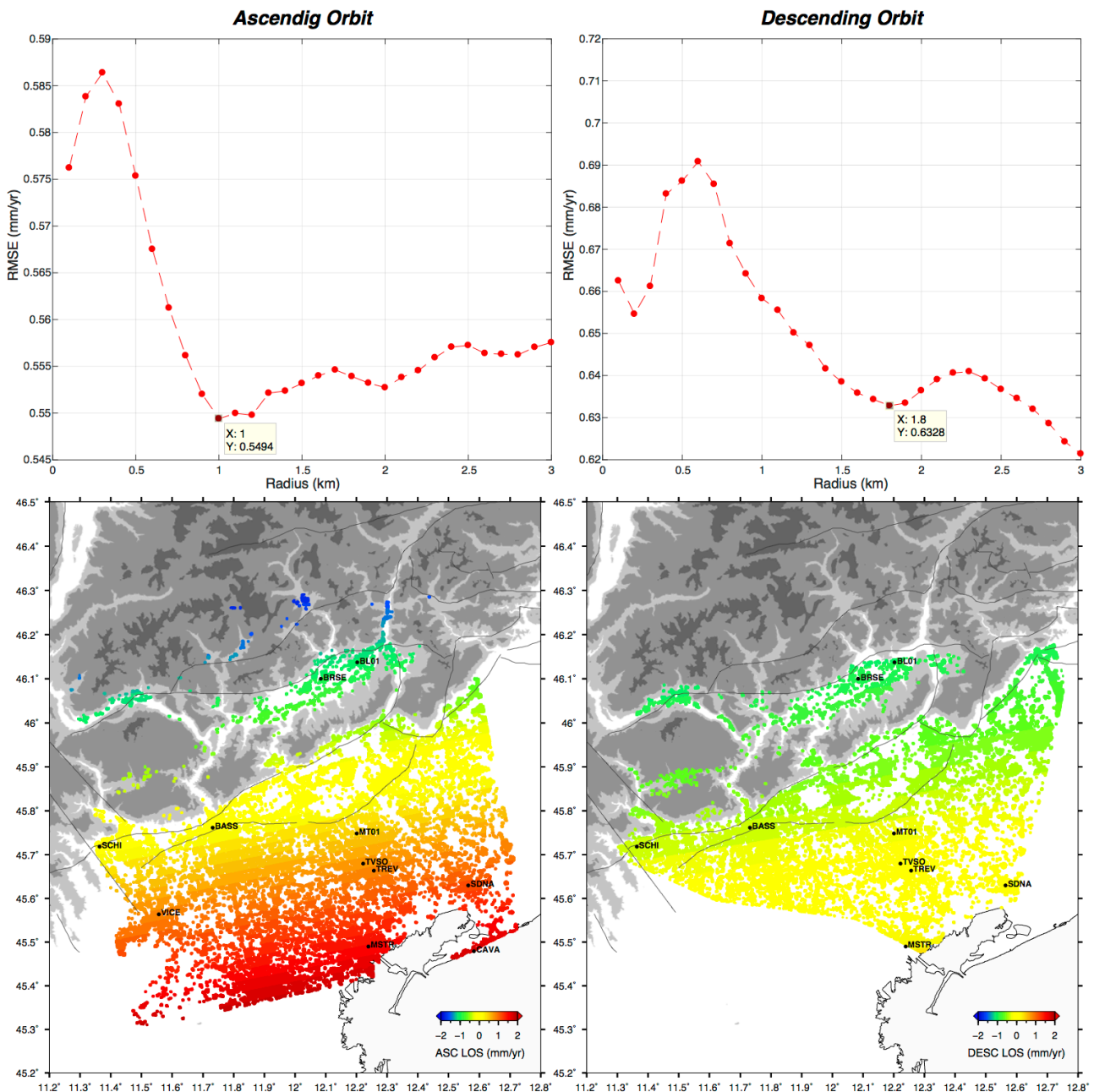


139

140

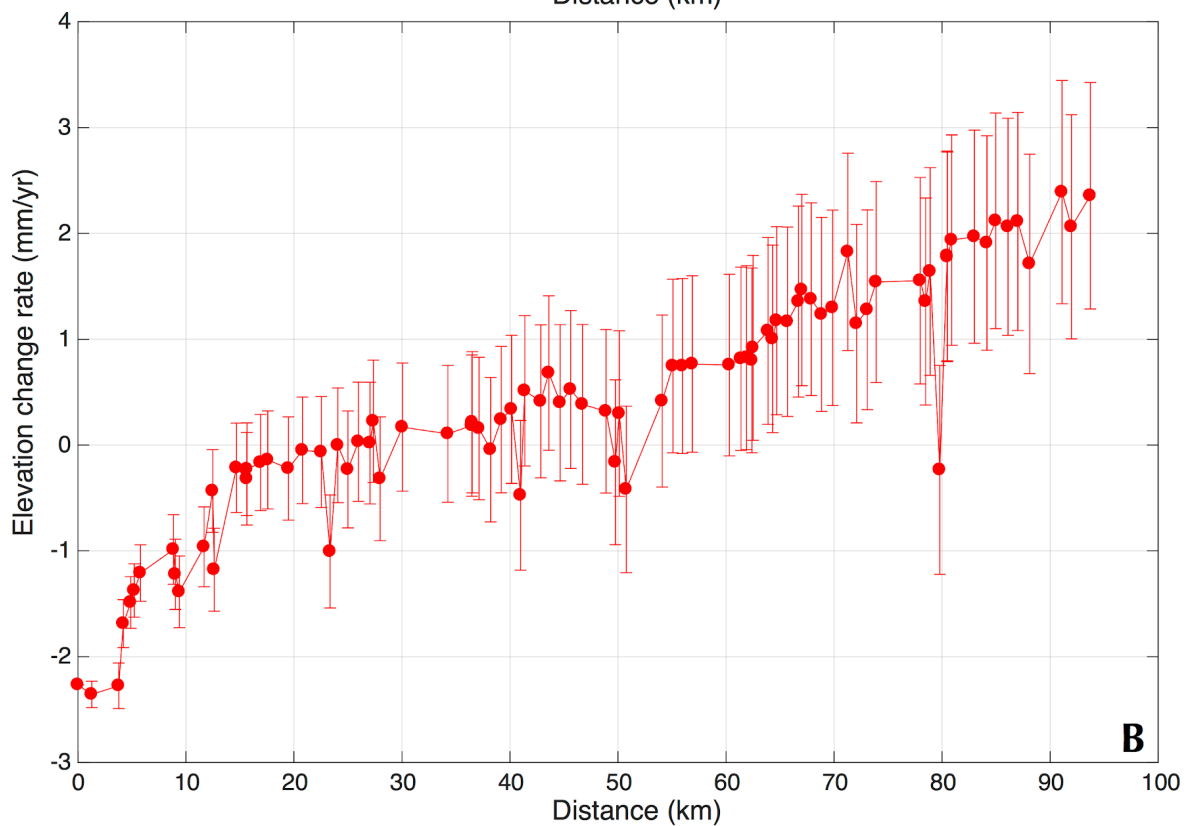
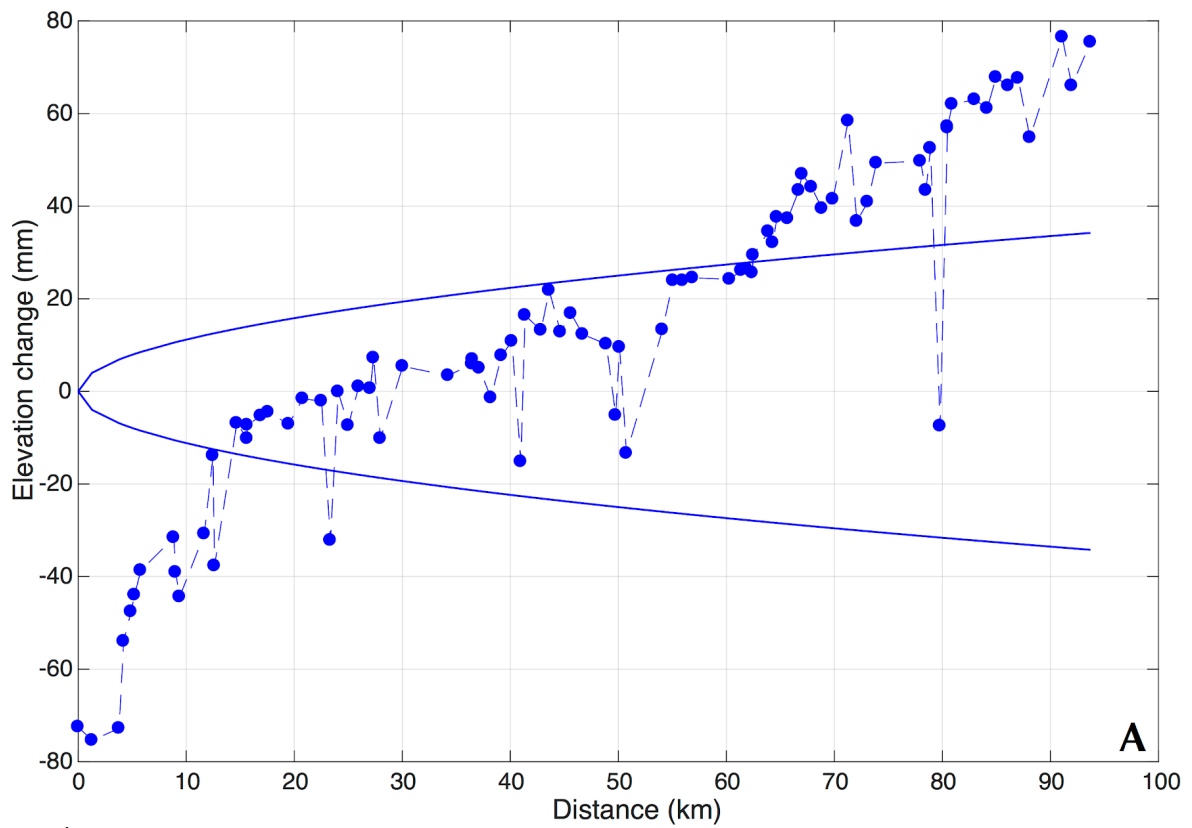
141 **Figure S1** InSAR line-of-sight (LOS) velocities for the ascending (left) and descending (right),  
 142 with negative (blue) and positive (red) values indicating increasing and decreasing distance between  
 143 the Earth surface and the satellite. Colored diamonds indicate the 3D GPS velocities projected along  
 144 the SAR LOS directions. Bottom panels show the SAR and GPS LOS velocities along the A-B cross  
 145 section (dashed box) for the ascending and descending orbits, respectively.

146



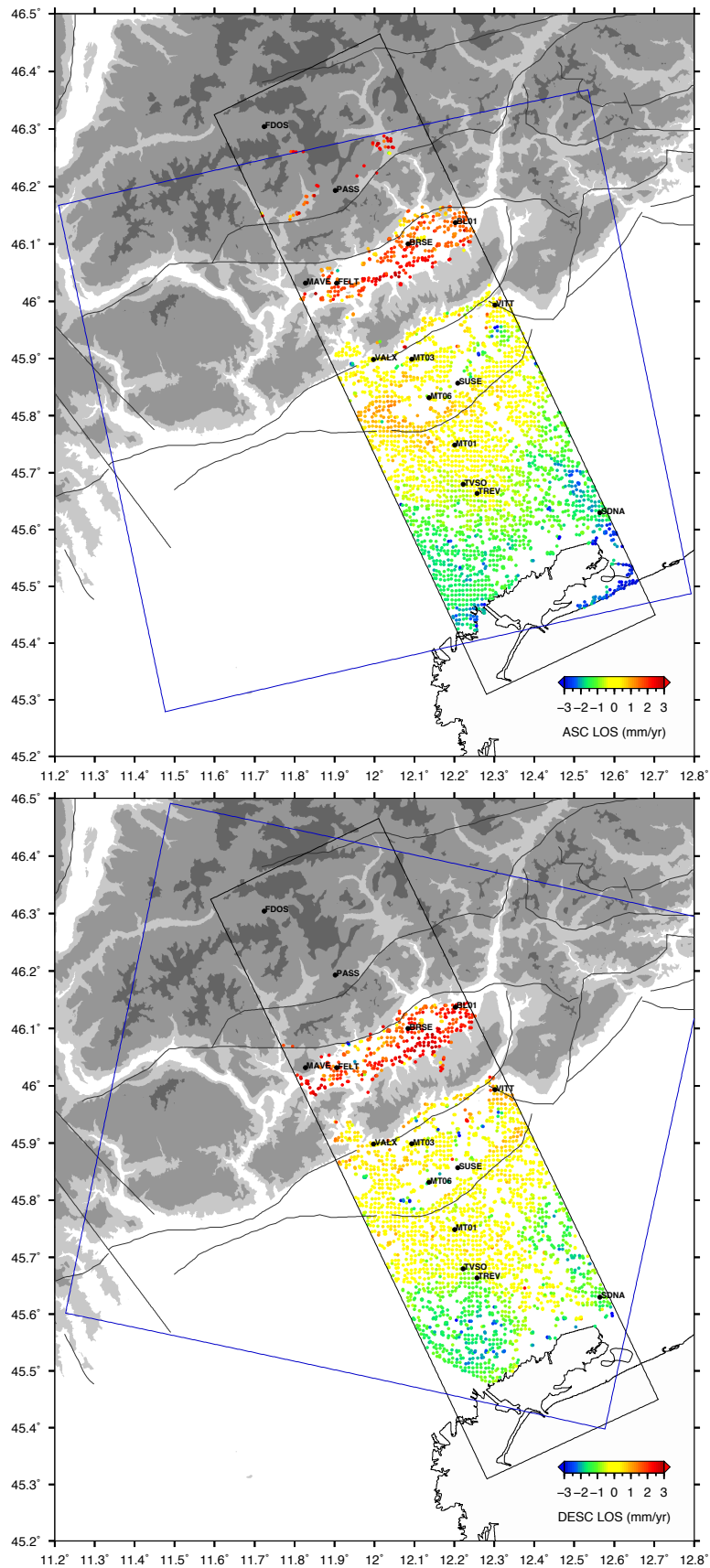
147  
 148  
 149  
 150  
 151  
 152  
 153  
 154  
 155  
 156  
 157  
 158

**Figure S2** Planar ramp correction for InSAR datasets - Top: RMSE estimate after the planar signal removal for the considered GPS stations (named sites in the bottom panels) varying the neighbouring radius and considering the mean value of InSAR velocities as representative of each point. We choose the radius for which we obtain the minimum of the RMSE, i.e. 1 km for the ascending dataset and 1.8 km for the descending one - Bottom: final planar ramp correction applied to the ascending (left) and descending (right) datasets.

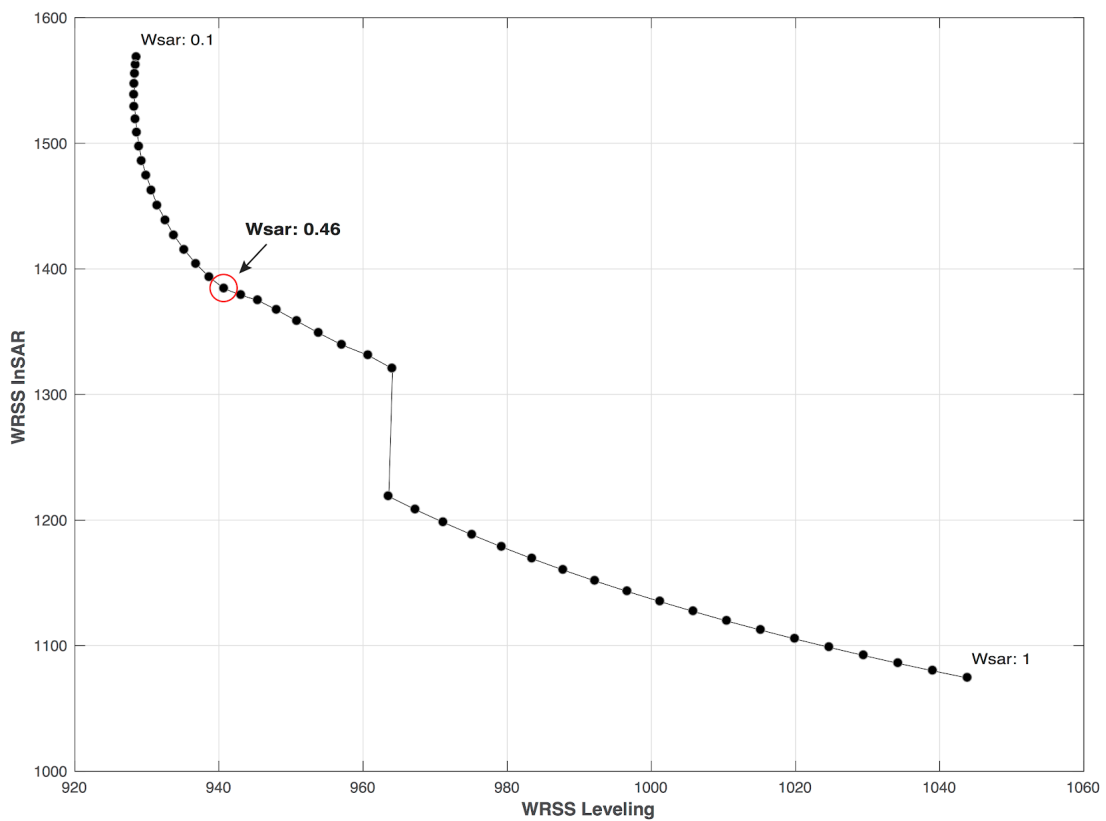
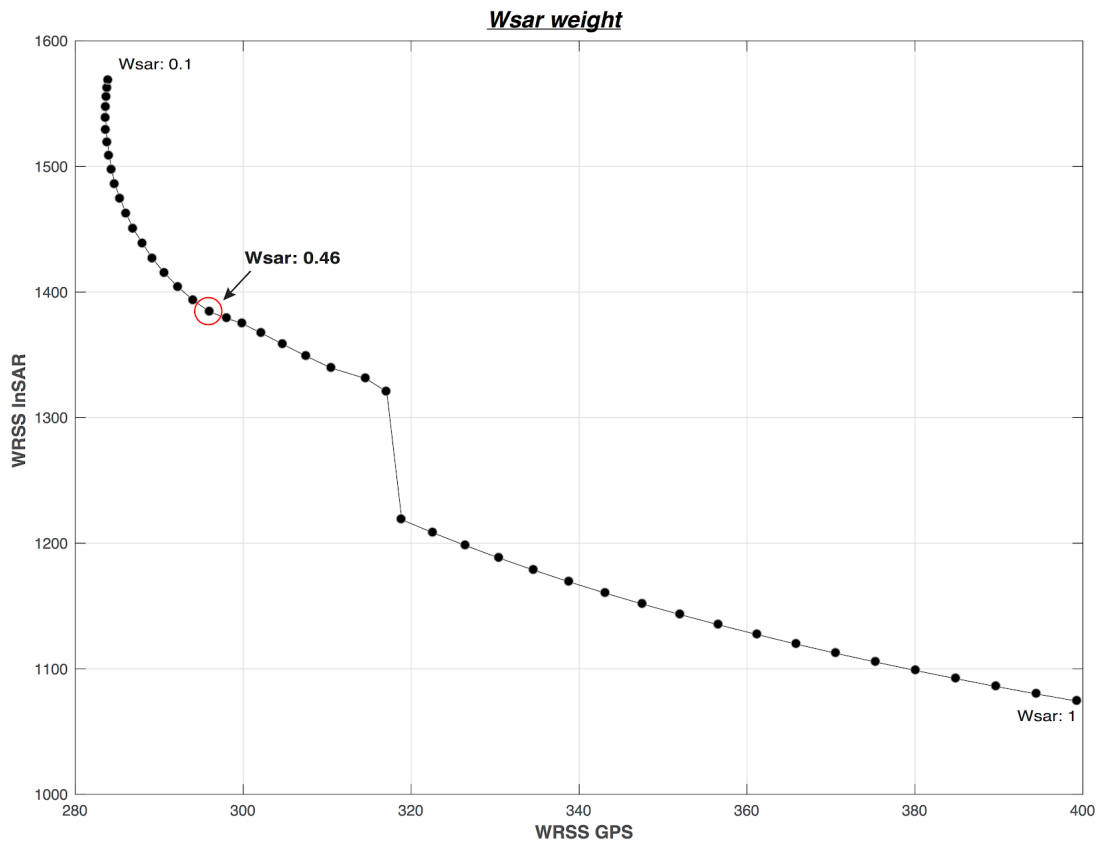


159  
 160 **Figure S3** A. Elevation change estimates along the leveling line measured in the time interval 1952-  
 161 1984 (EC values in Table S2), continuous lines indicate the maximum propagation error allowed  
 162 following the calculation indicated in Text S2 - B. Elevation change rates from leveling data with  
 163 associated errors (see Table S2).



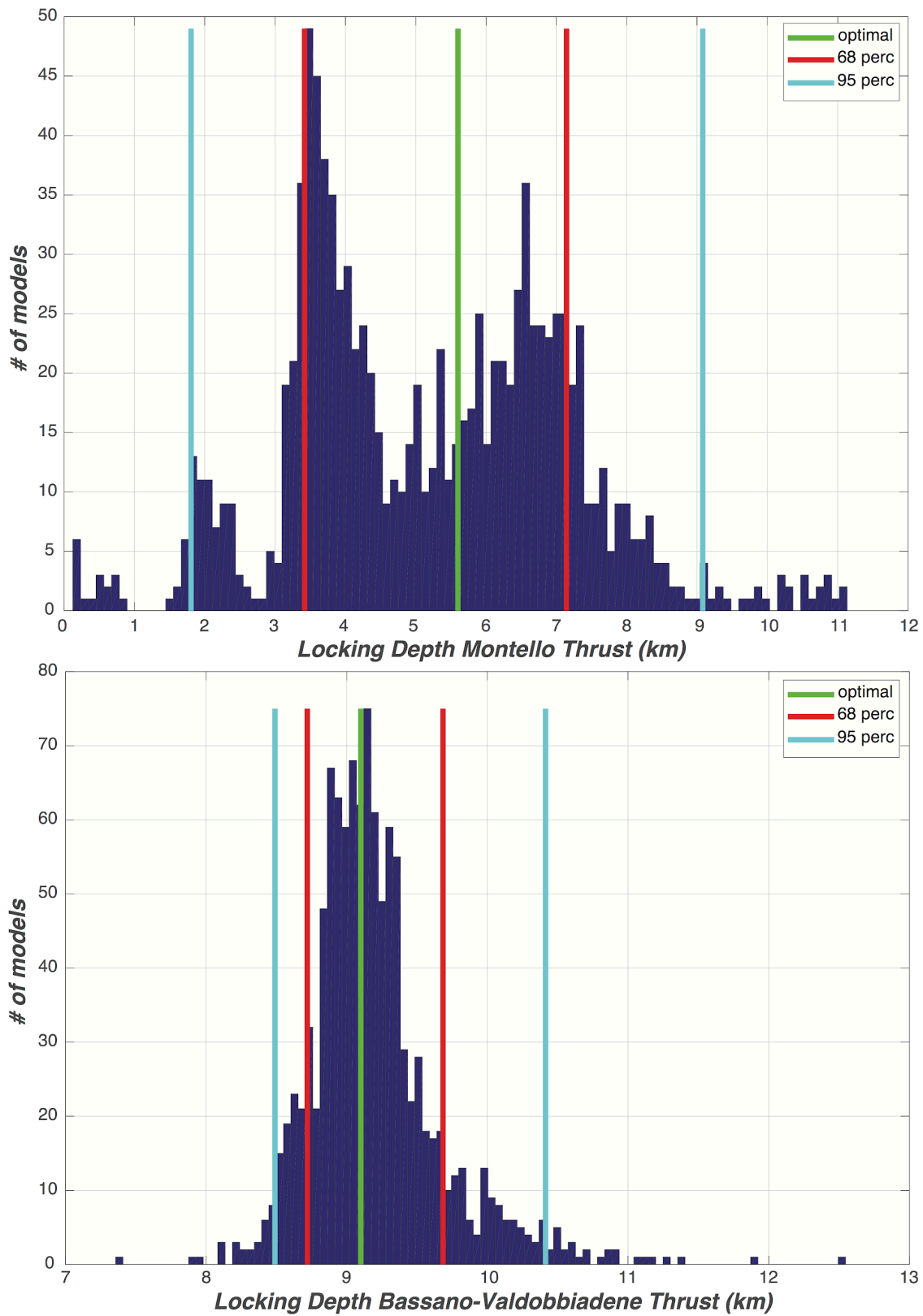


164  
 165 **Figure S4.** Subsampled DInSAR velocities for both the ascending (top) and descending (bottom)  
 166 datasets along a 35 km wide transect oriented towards NNW. The reported GPS sites are those used  
 167 for the dislocation modeling.



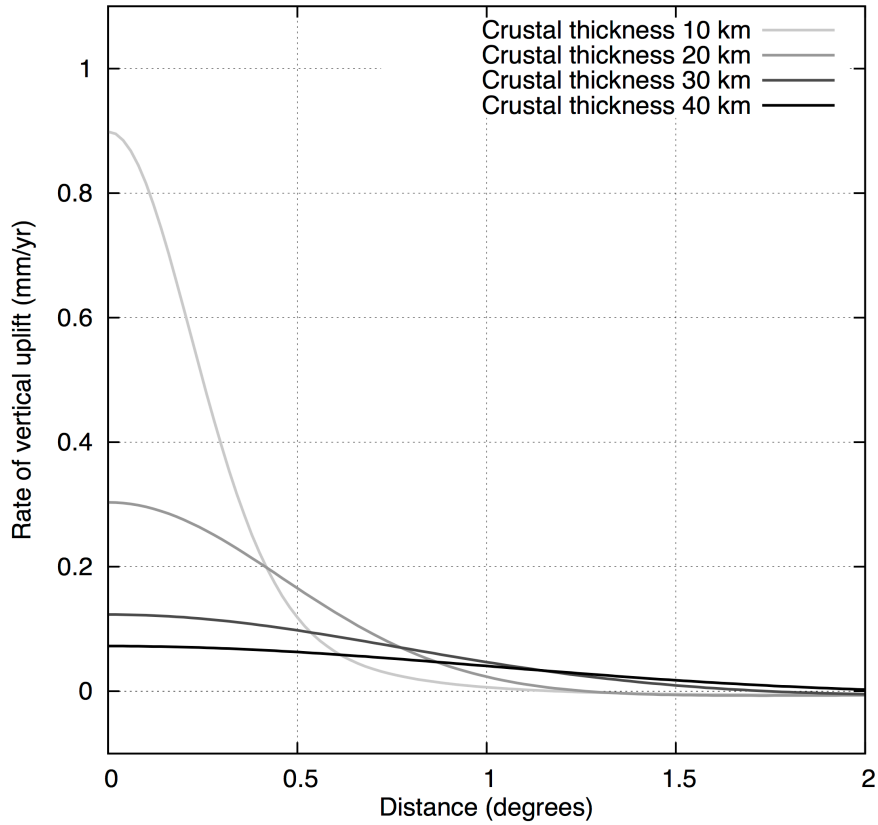
168

169 **Figure S5** Trade-off curves between Weighted Residuals Sum of Squares (WRSS) of GPS and  
 170 InSAR data (top) and Leveling and InSAR data (bottom) varying the weighting factor  $W_{sar}$  in the  
 171 interval  $[0.1-1]$  with steps of 0.02. The optimal value of  $W_{sar}$  0.46 has been chosen as the “knee  
 172 point” of the curves.



173

174 **Figure S6** Frequency histograms of modeled fault locking depths for the Montello ramp (top) and  
 175 the Bassano-Valdobbiadene thrust (bottom) obtained from 1000 bootstrap resamples (e.g. Árnadóttir  
 176 and Segall 1994) of the InSAR and GPS data. Green lines mark the estimated values of each  
 177 parameter. Light blue and red lines mark lower and upper bounds values at 95 and 68 percentile  
 178 confidence level, respectively.



179

180 **Figure S7:** Vertical velocities due to the Piave ice pond melting instantly 10 Kyr ago, modeled as a  
 181 disk, with a cap profile, of an equivalent area of  $\sim 45 \times 15 \text{ km}^2$ , 800 m thick. We used an Earth model  
 182 composed by a crustal layer, a viscosity profile consistent with the ICE5G model (VM2 of Peltier,  
 183 2004), with viscosity values of 2.7, 0.5 and  $0.5 \cdot 10^{21}$  Pa.s in the lower mantle, transition zone and  
 184 upper mantle, respectively. The model is run at harmonic degrees up to 6000.

185

186

187 **Table S1:** Horizontal and vertical GPS velocities in a Adria-fixed reference frame.

188

	lon	lat	Ve	Vn	Se	Sn	Ren	Vu	Su	Reu	Run	site	t1	t2
189	12.7990	46.4147	0.574	-1.243	0.032	0.051	-0.0063	0.820	0.176	0.0717	-0.1707	AMPE_GPS	1999.4013	2017.3821
190	11.5254	45.8663	0.077	-0.547	0.053	0.053	0.0353	-0.107	0.243	-0.0303	-0.1583	ASIA_GPS	2003.6013	2017.3821
191	12.5636	46.1931	-0.026	-0.636	0.096	0.093	-0.0570	-0.086	0.389	0.0739	-0.1616	BARC_GPS	2007.8369	2017.3821
192	11.7314	45.7618	0.520	-0.679	0.084	0.083	0.0011	0.182	0.197	0.0203	-0.1656	BASS_GPS	2007.7712	2014.7219
193	13.0694	45.6719	0.055	0.258	0.063	0.063	0.0077	-2.177	0.282	0.0005	-0.1178	BEVA_GPS	2008.0368	2017.3821
194	12.2025	46.1370	0.368	-0.822	0.070	0.082	-0.0109	1.520	0.176	0.0340	-0.1193	BL01_GPS	2008.1816	2017.3821
195	11.3652	46.4970	0.928	-0.546	0.138	0.121	0.0437	0.056	0.460	-0.0479	-0.0718	BOLZ_GPS	2012.0532	2017.3821
196	11.2842	45.4007	0.091	-0.422	0.113	0.169	0.0132	-0.753	0.406	0.0391	-0.1352	BONI_GPS	2012.0915	2016.9275
197	11.9694	45.5329	0.073	-0.213	0.103	0.092	0.0016	0.427	0.730	0.0178	-0.1010	BOR2_GPS	2008.4713	2014.9191
198	12.2181	46.4372	0.578	-0.924	0.115	0.102	0.1121	0.933	0.312	-0.1024	-0.2098	BORC_GPS	2009.2260	2017.3821
199	11.0343	45.5998	0.110	-0.154	0.071	0.071	-0.0009	-0.080	0.220	0.0468	-0.1263	BOSC_GPS	2006.1739	2016.9467
200	12.0841	46.1000	0.286	-1.058	0.115	0.135	-0.0295	1.943	0.328	0.0634	-0.1434	BRSE_GPS	2008.7855	2017.3821
201	11.2783	45.2578	-0.169	-0.616	0.070	0.083	-0.0050	-1.811	0.334	0.0207	-0.1014	BTAC_GPS	2008.6243	2017.3821
202	11.3368	46.4990	0.574	-0.804	0.043	0.048	-0.0544	0.987	0.132	0.0283	-0.0740	BZRG_GPS	1998.0013	2017.3821
203	11.9392	45.6703	0.140	-0.190	0.131	0.089	0.0092	-0.771	0.280	0.0255	-0.1286	CAFV_GPS	2011.1657	2017.3821
204	12.4350	46.0083	0.363	-0.793	0.115	0.125	-0.0716	-0.051	0.161	0.1306	-0.1663	CANV_GPS	2004.3838	2017.3821
205	12.5827	45.4794	-0.061	0.498	0.049	0.059	-0.0351	-2.805	0.208	0.0413	-0.1173	CAVA_GPS	2001.5438	2011.1657
206	12.2655	45.2065	-0.200	-0.262	0.202	0.093	0.0136	-3.373	0.399	0.0212	-0.1334	CGIA_GPS	2010.9630	2017.3821

207	11.2814	45.5427	0.219	0.029	0.140	0.190	0.0608	0.028	0.409	0.0481	-0.1118	CHI9_GPS	2012.0833	2017.3767
208	11.7946	45.6395	0.199	0.090	0.091	0.073	-0.0042	-2.571	0.358	0.0301	-0.1289	CITD_GPS	2009.1520	2017.3821
209	12.9791	45.9585	0.026	0.061	0.054	0.064	-0.0146	-0.624	0.188	0.0301	-0.1330	CODR_GPS	2007.3767	2017.3821
210	11.7238	46.3039	0.430	-0.779	0.049	0.085	-0.0243	0.893	0.179	0.0217	-0.0821	FDOS_GPS	2006.1657	2017.3821
211	11.9055	46.0318	0.832	-1.460	0.207	0.206	-0.0032	1.307	0.393	0.0322	-0.1125	FELT_GPS	2012.0751	2017.3821
212	13.0011	46.4142	0.557	-1.109	0.058	0.083	-0.0579	0.576	0.230	0.1522	-0.1776	FUSE_GPS	2007.6917	2017.3821
213	12.3850	45.9284	0.152	-0.041	0.097	0.208	0.0116	-1.213	0.417	0.0206	-0.1366	GOD9_GPS	2012.0860	2017.3821
214	13.4161	46.1840	0.168	-0.549	0.057	0.053	-0.0157	-0.079	0.168	0.0207	-0.1297	JOAN_GPS	2007.4890	2017.3821
215	11.2685	45.1841	0.162	0.208	0.078	0.084	-0.0282	-1.705	0.201	0.0258	-0.1286	LEGN_GPS	2008.6516	2016.1898
216	11.6691	45.7483	0.314	-0.377	0.123	0.101	0.0135	-0.749	0.353	0.0115	-0.1527	MARO_GPS	2012.0833	2017.3821
217	11.8271	46.0321	0.236	-0.065	0.097	0.086	-0.0116	-0.161	0.236	0.0371	-0.1188	MAVE_GPS	2006.3794	2016.9986
218	13.4356	45.9245	-0.043	0.199	0.035	0.028	-0.0705	-0.283	0.138	0.1068	-0.1859	MDEA_GPS	2003.0643	2017.3821
219	12.0151	45.9753	0.303	-0.332	0.110	0.165	-0.0273	-0.259	0.337	0.0157	-0.1182	MGRD_GPS	2009.6917	2017.3821
220	12.0954	45.4976	0.078	0.169	0.133	0.119	0.0117	-0.444	0.352	0.0217	-0.1284	MIRA_GPS	2012.4658	2017.3821
221	11.1434	46.0981	0.618	-0.371	0.050	0.051	-0.0195	0.949	0.174	0.0391	-0.1246	MOCA_GPS	2006.6972	2017.3821
222	13.1983	46.4067	0.340	-1.018	0.035	0.070	0.0343	0.783	0.148	-0.0603	-0.1809	MOGG_GPS	1999.4013	2017.3767
223	12.9877	46.2408	0.054	-0.679	0.061	0.089	-0.0438	-0.038	0.134	0.0967	-0.2029	MPRA_GPS	2003.0205	2017.3821
224	12.2386	45.4904	-0.244	0.165	0.064	0.107	0.0063	-2.493	0.338	0.0617	-0.1274	MSTR_GPS	2007.8890	2014.6342
225	12.2006	45.7487	-0.033	0.300	0.056	0.077	-0.0138	0.205	0.242	0.0175	-0.1300	MT01_GPS	2009.2178	2017.3821
226	12.1699	45.8403	0.071	-0.989	0.149	0.202	0.0878	-1.694	0.822	-0.2207	-0.2608	MT02_GPS	2009.2150	2014.5657
227	12.0934	45.8988	0.055	-0.458	0.156	0.200	-0.0038	1.004	0.529	0.0431	-0.1781	MT03_GPS	2009.4260	2015.4972
228	12.1364	45.8313	0.587	-0.974	0.121	0.186	0.0262	0.433	0.877	0.0069	-0.1539	MT06_GPS	2012.0532	2017.3821
229	12.5884	45.6684	0.968	-0.432	0.120	0.140	-0.0043	-3.217	0.287	0.0253	-0.1335	NOVE_GPS	2009.4013	2017.3821
230	12.4891	45.7878	0.020	0.169	0.072	0.124	0.0112	-1.259	0.298	0.0203	-0.1362	ODEZ_GPS	2011.1712	2017.3821
231	11.8961	45.4112	0.128	-0.391	0.042	0.064	-0.0258	-0.319	0.103	0.0259	-0.0949	PADO_GPS	2001.9054	2017.3821
232	11.1230	45.7769	0.409	-0.277	0.102	0.095	0.1243	0.061	0.270	-0.0415	-0.1671	PARR_GPS	2006.7794	2017.3821
233	11.9020	46.1930	0.133	-0.931	0.110	0.112	-0.1025	0.735	0.247	0.0529	-0.0553	PASS_GPS	2006.9767	2017.3821
234	13.0526	45.8057	-0.031	-0.276	0.043	0.045	-0.0227	0.169	0.181	0.0281	-0.0951	PAZO_GPS	2007.9301	2017.3821
235	11.8793	45.4222	-0.173	-0.198	0.235	0.198	-0.0141	-0.165	0.904	0.0519	-0.1150	PD01_GPS	2007.8506	2010.4890
236	13.3076	45.9046	-0.285	-0.200	0.043	0.044	-0.0039	0.096	0.120	0.0070	-0.1044	PLMN_GPS	1999.4972	2012.8811
237	12.6612	45.9568	-0.023	0.041	0.042	0.053	-0.0120	-0.021	0.140	0.0230	-0.0829	PORD_GPS	2002.0013	2017.3821
238	12.8331	45.7674	0.531	0.284	0.057	0.063	-0.0191	-2.726	0.245	0.0316	-0.1250	PORT_GPS	2007.5273	2017.3821
239	11.6817	46.4226	0.648	-0.891	0.086	0.082	-0.1284	0.862	0.231	0.0795	-0.1791	POZZ_GPS	2006.7794	2017.3821
240	12.0299	45.1959	0.255	-0.123	0.079	0.082	0.0213	-0.902	0.232	0.0007	-0.1540	REBO_GPS	2010.3794	2017.2917
241	11.0421	45.8935	0.164	-0.357	0.055	0.054	-0.0421	0.262	0.229	0.0640	-0.1741	ROVE_GPS	2004.1898	2017.3821
242	11.0721	45.6469	0.226	-0.350	0.101	0.079	-0.0393	0.107	0.251	0.0039	-0.1220	ROVR_GPS	2008.7718	2017.3821
243	12.3365	45.4307	0.418	0.069	0.195	0.149	0.0065	-0.950	0.516	0.0202	-0.1396	SAL_GPS	2014.3931	2017.3821
244	11.1416	46.4187	0.811	-0.501	0.055	0.051	-0.0184	1.306	0.192	0.0310	-0.1229	SARN_GPS	2006.8287	2017.3821
245	11.3630	45.7181	0.089	0.049	0.070	0.088	-0.0239	0.126	0.284	0.0382	-0.1394	SCHI_GPS	2008.3920	2017.3821
246	12.5642	45.6298	0.127	-0.189	0.061	0.101	-0.0138	-0.247	0.285	0.0257	-0.0855	SDNA_GPS	2007.4863	2017.3794
247	11.8020	45.6006	0.253	0.063	0.106	0.145	0.0100	-1.177	0.396	0.0240	-0.1371	SGIO_GPS	2012.0833	2017.3821
248	11.5094	46.0694	0.177	-0.750	0.060	0.088	-0.0195	0.863	0.203	0.0213	-0.1687	SPER_GPS	2006.7794	2017.3821
249	12.2085	45.8570	0.216	-0.299	0.122	0.108	0.0333	-0.686	0.520	0.0686	-0.1755	SUSE_GPS	2011.1383	2017.3821
250	12.3961	46.0605	0.458	-0.216	0.165	0.218	0.0099	-0.161	0.707	0.0459	-0.1486	TAMB_GPS	2011.6808	2017.3821
251	11.6773	45.3428	-0.240	0.056	0.045	0.044	-0.0412	-0.250	0.208	0.0409	-0.1112	TEOL_GPS	2004.2472	2017.3821
252	11.1102	46.1023	0.287	0.290	0.128	0.113	0.0324	0.729	0.418	0.0426	-0.1754	TRE8_GPS	2012.0532	2017.3821
253	12.2217	45.6798	0.111	0.070	0.121	0.120	0.0129	-1.254	0.372	0.0150	-0.1398	TRE9_GPS	2012.0833	2017.3821
254	11.1183	46.0909	0.761	-0.619	0.082	0.079	0.0387	-0.187	0.215	-0.0518	-0.2216	TREN_GPS	2006.7794	2017.3821
255	12.2565	45.6639	-0.182	-0.135	0.075	0.069	-0.0182	0.176	0.251	0.0507	-0.1054	TREV_GPS	2004.3319	2011.1657
256	12.2432	45.6532	-0.053	0.322	0.100	0.102	0.0176	-0.823	0.367	0.0091	-0.1282	TREX_GPS	2011.1712	2017.3821
257	12.2217	45.6798	0.020	-0.016	0.072	0.080	-0.0426	-0.968	0.230	0.0512	-0.1344	TVSO_GPS	2008.6489	2017.3821
258	13.2530	46.0375	-0.064	-0.174	0.047	0.052	-0.0229	-0.161	0.183	0.0369	-0.1337	UDI1_GPS	2006.2561	2017.3821
259	13.2277	46.0552	0.192	0.027	0.083	0.098	0.0002	-0.201	0.278	0.0293	-0.1220	UDI2_GPS	2008.3265	2017.3821
260	13.2530	46.0372	-0.135	0.816	0.170	0.280	0.0020	0.211	0.564	0.0292	-0.0677	UDIN_GPS	2003.0205	2006.6780
261	13.2165	46.0831	-0.129	-0.217	0.073	0.080	0.0259	0.313	0.415	-0.0630	-0.1904	UNUD_GPS	2006.1821	2017.3821
262	11.8779	45.4067	0.222	0.156	0.151	0.185	-0.0871	0.712	0.419	0.0213	-0.0941	UPAD_GPS	1995.0945	2001.8890
263	11.9976	45.8982	0.068	-0.720	0.143	0.193	0.0560	0.028	0.456	-0.0232	-0.2067	VALX_GPS	2011.1712	2017.3821
264	12.5653	46.4571	0.757	-0.922	0.295	0.164	-0.0150	0.144	1.470	0.0210	-0.1326	VARM_GPS	2014.0068	2017.3821
265	12.3578	45.4379	-0.129	0.244	0.138	0.147	-0.0042	-2.273	0.686	-0.0783	-0.2545	VEAR_GPS	2006.1602	2010.7164
266	11.3667	45.7887	0.222	-0.549	0.097	0.090	0.0772	0.008	0.356	0.0946	-0.0457	VELO_GPS	2009.3493	2017.3821
267	12.3541	45.4306	0.110	-0.566	0.067	0.100	-0.0318	-1.550	0.213	0.0170	-0.1255	VEN1_GPS	2009.8068	2017.3821

268 11.0024 45.4447 0.146 -0.480 0.060 0.088 -0.0156 -0.242 0.190 0.0324 -0.0916 VERO\_GPS 2006.8013 2017.3821  
 269 11.5563 45.5641 0.116 -0.254 0.047 0.063 -0.0361 -0.620 0.264 0.0472 -0.1291 VICE\_GPS 2008.6489 2017.3821  
 270 12.3014 45.9933 0.506 -0.721 0.116 0.141 0.0186 0.378 0.347 0.0204 -0.1857 VITT\_GPS 2011.1849 2017.3821  
 271 11.9109 45.3846 -0.163 0.249 0.051 0.050 -0.0285 0.032 0.394 0.0351 -0.1265 VOLT\_GPS 2001.5575 2011.1657  
 272  
 273

274

275 **Table S2:** Vertical ground motion rates (i.e Elevation Change, EC, rates) estimated from the IGM  
 276 elevation measurements performed in the 1952-3 and in the 1984-5 leveling campaigns, where *nbc*  
 277 *m* is the benchmark number, *dist* indicates the distance from the first benchmark and the errors have  
 278 been calculated following the formulas presented in Text S2.

<b>nbc</b>	<b>m</b>	<b>dist</b> (km)	<b>long</b>	<b>lat</b>	<b>1952-3</b> (m)	<b>1984-5</b> (m)	<b>EC</b> (mm)	<b>EC error</b> (mm)	<b>EC_rate</b> (mm/yr)	<b>EC_rate_sig</b> (mm/yr)
0	0	0	12.2233	45.4764	3.9672	3.8947	-72.50	0.0000	-2.2656	0.0000
1	1	1.28	12.2222	45.4858	5.0708	4.9954	-75.40	4.0000	-2.3563	0.1250
2	2	3.78	12.238	45.5006	2.8441	2.7713	-72.80	6.8739	-2.2750	0.2148
3	3	4.21	12.2386	45.5061	4.2709	4.2169	-54.00	7.2543	-1.6875	0.2267
4	4	4.89	12.2388	45.5106	5.8518	5.8042	-47.60	7.8182	-1.4875	0.2443
5	5	5.22	12.2391	45.5139	4.1567	4.1127	-44.00	8.0777	-1.3750	0.2524
6	6	5.79	12.2386	45.5178	6.9893	6.9506	-38.70	8.5073	-1.2094	0.2659
7	7	8.85	12.2366	45.5442	6.8699	6.8383	-31.60	10.5178	-0.9875	0.3287
8	8	9.02	12.2358	45.5494	6.0162	5.9771	-39.10	10.6184	-1.2219	0.3318
9	9	9.39	12.2352	45.5528	8.4444	8.4	-44.40	10.8340	-1.3875	0.3386
10	10	11.68	12.2358	45.5692	8.0962	8.0654	-30.80	12.0830	-0.9625	0.3776
11	11	12.48	12.2341	45.5778	8.4539	8.44	-13.90	12.4900	-0.4344	0.3903
12	12	12.62	12.2338	45.5778	9.265	9.2273	-37.70	12.5599	-1.1781	0.3925
13	13	14.68	12.2358	45.5958	13.4197	13.4128	-6.90	13.5462	-0.2156	0.4233
14	14	15.64	12.2344	45.6028	14.8071	14.7969	-10.20	13.9821	-0.3188	0.4369
15	15	15.65	12.2344	45.6028	14.9285	14.9212	-7.30	13.9866	-0.2281	0.4371
16	16	16.91	12.2372	45.6083	10.813	10.8077	-5.30	14.5387	-0.1656	0.4543
17	17	17.58	12.2391	45.6186	11.2075	11.203	-4.50	14.8240	-0.1406	0.4632
18	18	19.49	12.2411	45.6358	14.9831	14.976	-7.10	15.6085	-0.2219	0.4878
19	19	20.79	12.2444	45.6481	14.6418	14.6402	-1.60	16.1206	-0.0500	0.5038
20	20	22.53	12.2463	45.6656	17.0483	17.0462	-2.10	16.7817	-0.0656	0.5244
21	21	23.35	12.2561	45.6653	11.0334	11.0012	-32.20	17.0843	-1.0063	0.5339
22	22	24.07	12.2499	45.6708	16.0511	16.051	-0.10	17.3457	-0.0031	0.5421
23	23	25	12.2516	45.6789	14.4759	14.4685	-7.40	17.6777	-0.2313	0.5524
24	24	25.97	12.258	45.6883	18.4302	18.4312	1.00	18.0174	0.0313	0.5630
25	25	27.04	12.2597	45.695	19.8531	19.8537	0.60	18.3848	0.0188	0.5745
26	26	27.35	12.2599	45.6992	22.2282	22.2354	7.20	18.4899	0.2250	0.5778

27	27.98	12.2599	45.7036	22.8142	22.804	-10.20	18.7016	-0.3188	0.5844
28	30.04	12.2558	45.7214	28.8918	28.8972	5.40	19.3778	0.1688	0.6056
29	34.25	12.2522	45.7578	48.202	48.2054	3.40	20.6912	0.1063	0.6466
30	36.47	12.2586	45.7767	52.8135	52.8194	5.90	21.3512	0.1844	0.6672
31	36.51	12.2597	45.7769	56.4738	56.4807	6.90	21.3629	0.2156	0.6676
32	37.13	12.2594	45.7822	55.2555	55.2605	5.00	21.5436	0.1563	0.6732
33	38.21	12.2558	45.7914	58.1218	58.1204	-1.40	21.8546	-0.0438	0.6830
34	39.19	12.2536	45.8	64.4865	64.4942	7.70	22.1331	0.2406	0.6917
35	40.15	12.2505	45.8086	67.3459	67.3567	10.80	22.4026	0.3375	0.7001
36	40.98	12.2491	45.8142	72.4976	72.4824	-15.20	22.6329	-0.4750	0.7073
37	41.37	12.253	45.8178	72.9978	73.0142	16.40	22.7404	0.5125	0.7106
38	42.85	12.2572	45.83	67.5596	67.5728	13.20	23.1436	0.4125	0.7232
39	43.6	12.2558	45.8369	70.8439	70.8657	21.80	23.3452	0.6813	0.7295
40	44.65	12.2513	45.8453	74.7978	74.8106	12.80	23.6247	0.4000	0.7383
41	45.62	12.2513	45.8503	77.3346	77.3514	16.80	23.8799	0.5250	0.7462
42	46.71	12.2633	45.8589	64.9263	64.9386	12.30	24.1635	0.3844	0.7551
43	48.89	12.2805	45.8728	60.3113	60.3215	10.20	24.7209	0.3188	0.7725
44	49.76	12.2886	45.8789	58.8121	58.8069	-5.20	24.9399	-0.1625	0.7794
45	50.12	12.2908	45.8803	59.3332	59.3427	9.50	25.0300	0.2969	0.7822
46	50.76	12.2999	45.8839	63.9551	63.9417	-13.40	25.1893	-0.4188	0.7872
47	54.09	12.3302	45.9019	66.447	66.4603	13.30	26.0024	0.4156	0.8126
48	55.08	12.3255	45.9103	70.0553	70.0792	23.90	26.2393	0.7469	0.8200
49	55.96	12.3216	45.9175	75.2025	75.2264	23.90	26.4481	0.7469	0.8265
50	56.88	12.3224	45.9256	80.4213	80.4458	24.50	26.6646	0.7656	0.8333
51	60.31	12.3249	45.9553	103.1457	103.1699	24.20	27.4568	0.7563	0.8580
52	61.39	12.3249	45.9633	107.0572	107.0833	26.10	27.7015	0.8156	0.8657
53	61.9	12.3202	45.9653	107.4331	107.4595	26.40	27.8164	0.8250	0.8693
54	62.4	12.3147	45.9697	114.1532	114.1788	25.60	27.9285	0.8000	0.8728
55	62.5	12.3169	45.9675	112.8119	112.8413	29.40	27.9508	0.9188	0.8735
56	63.89	12.3083	45.9758	123.8826	123.9171	34.50	28.2600	1.0781	0.8831
57	64.31	12.3047	45.9814	127.7338	127.7659	32.10	28.3527	1.0031	0.8860
58	64.69	12.2961	45.9856	138.3567	138.3943	37.60	28.4363	1.1750	0.8886
59	65.69	12.2936	45.9931	143.6824	143.7197	37.30	28.6553	1.1656	0.8955
60	66.71	12.2919	46.0003	141.5122	141.5556	43.40	28.8769	1.3563	0.9024
61	67.02	12.2913	46.0031	141.5246	141.5715	46.90	28.9439	1.4656	0.9045
62	67.89	12.2888	46.0094	157.0616	157.1057	44.10	29.1312	1.3781	0.9103
63	68.85	12.2905	46.0181	164.6513	164.6908	39.50	29.3364	1.2344	0.9168
64	69.87	12.2955	46.0256	168.5418	168.5833	41.50	29.5529	1.2969	0.9235
65	71.28	12.3033	46.0306	186.9851	187.0435	58.40	29.8496	1.8250	0.9328

66	72.09	12.3111	46.0383	230.2242	230.2609	36.70	30.0187	1.1469	0.9381
67	73.08	12.3099	46.0433	286.2116	286.2525	40.90	30.2242	1.2781	0.9445
68	73.9	12.3149	46.05	285.9962	286.0455	49.30	30.3933	1.5406	0.9498
69	77.97	12.3349	46.0756	444.0567	444.1064	49.70	31.2190	1.5531	0.9756
70	78.48	12.3361	46.0775	427.211	427.2544	43.40	31.3209	1.3563	0.9788
71	78.9	12.3374	46.0792	489.1689	489.2214	52.50	31.4046	1.6406	0.9814
72	79.79	12.3358	46.0847	454.0982	454.0907	-7.50	31.5812	-0.2344	0.9869
73	80.48	12.333	46.0875	433.4771	433.5343	57.20	31.7175	1.7875	0.9912
74	80.49	12.333	46.0875	431.0088	431.0657	56.90	31.7195	1.7781	0.9912
75	80.9	12.3299	46.0919	407.2951	407.3571	62.00	31.8002	1.9375	0.9938
76	82.99	12.3274	46.1092	390.602	390.665	63.00	32.2083	1.9688	1.0065
77	84.15	12.3241	46.1178	395.9218	395.9829	61.10	32.4326	1.9094	1.0135
78	84.97	12.3197	46.1253	386.2923	386.3601	67.80	32.5903	2.1188	1.0184
79	86.1	12.318	46.135	385.2408	385.3068	66.00	32.8062	2.0625	1.0252
80	87.01	12.3199	46.1447	385.5099	385.5775	67.60	32.9792	2.1125	1.0306
81	88.11	12.3202	46.1522	387.5125	387.5673	54.80	33.1870	1.7125	1.0371
82	91.1	12.303	46.1733	391.7877	391.8642	76.50	33.7454	2.3906	1.0545
83	91.98	12.2938	46.1728	398.1984	398.2644	66.00	33.9080	2.0625	1.0596
84	93.72	12.2833	46.1789	402.5926	402.668	75.40	34.2272	2.3563	1.0696

279

280

281

282 **Table S3:** Parameters used for the subsampling of the ascending and descending InSAR datasets,  
 283 whose definition is reported in Text S3

<b>Orbit</b>	<b><math>T_p</math></b>	<b><math>N_p</math></b>	<b><math>R</math></b>	<b><math>div_{lon}</math></b>	<b><math>div_{lat}</math></b>	<b><math>n_{crit}</math></b>	<b><math>final\ pixel</math></b>
Asc	101273	2500	25%	10	10	1000	2679
Desc	85474	2500	38%	9	9	1050	2343

284

285

## 286 **References**

287 Altamimi, Z., Collilieux, X., Métivier, L., 2011. ITRF2008: an improved solution of the international  
 288 terrestrial reference frame. *J Geodesy* 85, 457–473. doi:10.1007/s00190-011-0444-4.

289 Árnadóttir, T., Segall, P., 1994. The 1989 Loma Prieta earthquake imaged from inversion of geodetic  
 290 data. *Journal of Geophysical Research: Solid Earth* 99, 21835–21855. doi:10.1029/94JB01256.

291 Blewitt, G., Lavallée, D., 2002. Effect of annual signals on geodetic velocity. *J Geophys Res* 107,  
 292 2145. doi:10.1029/2001JB000570.



293 Boehm, J., Werl, B., Schuh, H., 2006. Troposphere mapping functions for GPS and very long baseline  
 294 interferometry from European Centre for Medium-Range Weather Forecasts operational analysis  
 295 data. *J Geophys Res* 111. doi:10.1029/2005JB003629.

296 D'Anastasio, E., DeMartini, P.M., Selvaggi, G., Pantosti, D., Marchioni, A., Maseroli, R., 2006.  
 297 Short-term vertical velocity field in the Apennines (Italy) revealed by geodetic levelling data.  
 298 *Tectonophysics* 418, 219–234, doi:10.1016/j.tecto.2006.02.008

299 Dong, D., Herring, T., King, R., 1998. Estimating regional deformation from a combination of space  
 300 and terrestrial geodetic data. *J Geodesy* 72, 200–214.

301 Dong, D., Fang, P., Bock, Y., Cheng, M., Miyazaki, S., 2002. Anatomy of apparent seasonal  
 302 variations from GPS-derived site position time series. *J Geophys Res-Sol Ea* 107, –.  
 303 doi:10.1029/2001JB000573.

304 Dong, D., Fang, P., Bock, Y., Webb, F., Prawirodirdjo, L., Kedar, S., Jamason, P., 2006.  
 305 Spatiotemporal filtering using principal component analysis and Karhunen-Loeve expansion  
 306 approaches for regional GPS network analysis. *Journal of Geophysical Research: Solid Earth* 111,  
 307 doi:10.1029/2005JB003806

308 Herring, T. A., King, R. W., Floyd, M. A., McClusky, S. C., 2015. Introduction to GAMIT/GLOBK,  
 309 Release 10.6. Retrieved from [http://www-gpsg.mit.edu/~simon/gtgk/Intro\\_GG.pdf](http://www-gpsg.mit.edu/~simon/gtgk/Intro_GG.pdf).

310 Lagler, K., Schindelegger, M., Böhm, J., Krásná, H., & Nilsson, T. (2013). GPT2: Empirical slant  
 311 delay model for radio space geodetic techniques. *Geophysical Research Letters*, 40, 1069–1073.  
 312 <https://doi.org/10.1002/grl.50288>.

313 Lyard, F., Lefevre, F., Letellier, T., & Francis, O. (2006). Modelling the global ocean tides: Modern  
 314 insights from FES2004. *Ocean Dynamics*, 56(5-6), 394–415. [https://doi.org/10.1007/s10236-006-](https://doi.org/10.1007/s10236-006-0086-x)  
 315 [0086-x](https://doi.org/10.1007/s10236-006-0086-x) .

316 Peltier, W.R. 2004. Global glacial isostasy and the surface of the ice-age Earth: the ICE-5G (VM2)  
 317 model and GRACE. *Annual Review of Earth and Planetary Sciences* 2004 32:1, 111-149,  
 318 doi:10.1146/annurev.earth.32.082503.144359.

319 Schmid, R., Rothacher, M., Thaller, D., Steigenberger, P., 2005. Absolute phase center corrections  
 320 of satellite and receiver antennas. *GPS Solut* 9, 283–293. doi:10.1007/s10291-005-0134-x.

321 Schmid, R., Steigenberger, P., Gendt, G., Ge, M., Rothacher, M., 2007. Generation of a consistent  
 322 absolute phase-center correction model for GPS receiver and satellite antennas. *J Geodesy* 81, 781–  
 323 798. doi:10.1007/s00190-007-0148-y.

324 Serpelloni, E., Casula, G., Galvani, A., Anzidei, M., Baldi, P., 2006. Data analysis of permanent GPS  
 325 networks in Italy and surrounding regions: application of a distributed processing approach. *Ann*  
 326 *Geophys-Italy* 49, 897–928.

327 Serpelloni, E., Faccenna, C., Spada, G., Dong, D., Williams, S.D.P., 2013. Vertical GPS ground  
328 motion rates in the Euro-Mediterranean region: New evidence of velocity gradients at different spatial  
329 scales along the Nubia-Eurasia plate boundary. *J Geophys Res-Sol Ea* 118, 6003–6024.  
330 doi:10.1002/2013JB010102.

331 Vignal, J., 1936. Evaluation de la precision d'une methode de nivellement. *Bull. Geod.*, 49, 1–159.

332 Vignal, J., 1950. Comptes rendus des séances de travail de la Secion II. Nivellements, de l'Association  
333 Internationale de Géodésie à l'Assemblée Générale d'Oslo (Aout 1948). *Bull. Géod.* 18, 401–565.

334

335